Rapid Communications

Two-temperature scales in the triangular-lattice Heisenberg antiferromagnet

Lei Chen,[1] Dai-Wei Qu,[1] Han Li,[1] Bin-Bin Chen,[1,2] Shou-Shu Gong,[1] Jan von Delft,[2] Andreas Weichselbaum,[3,2,*] and Wei Li[1,4,†]

[1]*Department of Physics, Key Laboratory of Micro-Nano Measurement-Manipulation and Physics (Ministry of Education), Beihang University, Beijing 100191, China*

[2]*Munich Center for Quantum Science and Technology (MCQST), Arnold Sommerfeld Center for Theoretical Physics (ASC) and Center for NanoScience (CeNS), Ludwig-Maximilians-Universität München, Fakultät für Physik, D-80333 München, Germany*

[3]*Department of Condensed Matter Physics and Materials Science, Brookhaven National Laboratory, Upton, New York 11973-5000, USA*

[4]*International Research Institute of Multidisciplinary Science, Beihang University, Beijing 100191, China*

(Received 11 December 2018; published 10 April 2019; corrected 16 January 2020)

The anomalous thermodynamic properties of the paradigmatic frustrated spin-1/2 triangular-lattice Heisenberg antiferromagnet (TLH) has remained an open topic of research over decades, both experimentally and theoretically. Here, we further the theoretical understanding based on the recently developed, powerful exponential tensor renormalization group method on cylinders and stripes in a quasi-one-dimensional (1D) setup, as well as a tensor product operator approach directly in 2D. The observed thermal properties of the TLH are in excellent agreement with two recent experimental measurements on the virtually ideal TLH material $Ba_8CoNb_6O_{24}$. Remarkably, our numerical simulations reveal two crossover temperature scales, at $T_l/J \sim 0.20$ and $T_h/J \sim 0.55$, with J the Heisenberg exchange coupling, which are also confirmed by a more careful inspection of the experimental data. We propose that in the intermediate regime between the low-temperature scale T_l and the higher one T_h, the "rotonlike" excitations are activated with a strong chiral component and a large contribution to thermal entropies. Bearing remarkable resemblance to the renowned roton thermodynamics in liquid helium, these gapped excitations suppress the incipient 120° order that emerges for temperatures below T_l.

DOI: 10.1103/PhysRevB.99.140404

Introduction. The triangular-lattice Heisenberg (TLH) model is arguably the most simple prototype of a frustrated quantum spin system. It has attracted wide attention since Anderson's famous proposal of a resonating valence bond (RVB) spin liquid state [1]. The competition between RVB liquid versus semiclassical Néel solid states raised great interest. After decades of research, it is now widely accepted that the TLH has noncollinear 120° order at $T = 0$, with a spontaneous magnetization [2], $m \simeq 0.205$ [3,4]. Nevertheless, the TLH has long been noticed to possess *anomalous* thermodynamic properties [5], in the sense that thermal states down to rather low-temperature regimes behave more as a system with no indication of an ordered ground state [6,7].

Bipartite-lattice Heisenberg antiferromagnets (AFs) such as the square-lattice Heisenberg (SLH) model, develop a semiclassical magnetic order at $T = 0$ which is "melted" at any finite temperature according to the Mermin-Wagner theorem [8]. Nevertheless, the ground-state Néel order strongly influences low-temperature thermodynamics in the so-called renormalized classical (RC) regime [9,10], where the spin-spin correlation length ξ increases exponentially as T decreases [11–14].

In contrast, the thermodynamics of the TLH strikingly differs in many respects from that of SLH. Based on high-temperature series expansion (HTSE) results, both models show c_V peaks at similar temperatures, $T_h \simeq 0.55$ (TLH) and $T_s \simeq 0.6$ (SLH). The SLH enters the RC regime for $T \lesssim T_s$ [11,12], whereas the TLH shows no signature for incipient order and possesses anomalously large entropies at temperatures below T_h [6].

The classical SLH and TLH models have a similar spin stiffness ρ_s, and thus a similar constant, $C_\xi \sim \rho_s$, in the correlation length, $\xi \sim \exp(\frac{C_\xi}{T})$, as well as in the static structure factor at the ordering wave vector, $S(K) \sim \exp(\frac{2C_\xi}{T})$, with $C_\xi = 2\pi\rho_s = 1.571$ (SLH) [15] and $C_\xi = 4\pi\rho_s = 1.748$ (TLH) [5,16,17] in units of spin coupling J. However, the constant C_ξ is significantly renormalized by quantum fluctuations. For the SLH, the constant is reduced by about 30% to $C_\xi \sim 1.13$, while in the TLH it is reduced by an order of magnitude down to $C_\xi \sim 0.1$ [5,6]. The energy scale $E_{\rm RC} \equiv 2C_\xi$ naturally represents the onset of RC behavior and thus incipient order. Recent sign-blessing bold diagrammatic Monte Carlo (BDMC) simulations still show that the thermal states down to the lowest accessible temperatures $T = 0.375$ "extrapolate" to a disordered ground state via a quantum-to-classical correspondence [7].

Here, we exploit two renormalization group (RG) techniques based on thermal tensor network states (TNSs) [18–20]: the exponential tensor RG (XTRG) which we recently introduced based on one-dimensional (1D) matrix product operators (MPOs) [20], and a tensor product operator

*weichselbaum@bnl.gov
†w.li@buaa.edu.cn

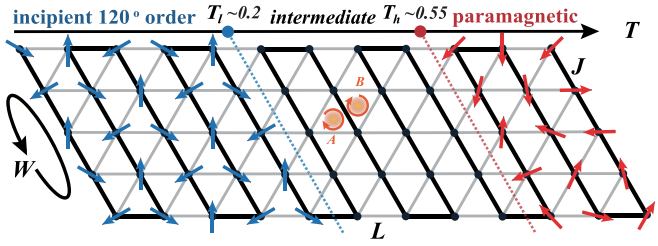

FIG. 1. Uniform TLH with nearest-neighbor (NN) coupling $J = 1$ (which thus sets the unit of energy) and lattice spacing $a = 1$, with three schematically depicted distinct regimes, separated by two crossover temperature scales, T_l and T_h: an incipient 120° ordered regime for $T < T_l$ (left), a paramagnetic regime for $T > T_h$ (right), an intermediate regime (center), which is explored in detail in this Rapid Communication. The thick black line indicates the 1D snake order adopted in the MPO-based XTRG. When the system is wrapped into a cylinder along the tilted left arrow, this is referred to as YC geometry. The clockwise oriented circles in the center of the system indicate chiral operators, $\chi \equiv 2^3 \cdot S_a \cdot (S_b \times S_c)$, acting on the enclosing triangle of sites (a, b, c) in the order of the arrows, as used for the calculation of chiral correlations between the triangle pair A-B.

(TPO) approach [18]. XTRG is employed to simulate the TLH down to temperatures $T < 0.1$ on YC $W(\times L)$ geometries (see Fig. 1) up to width $W = 6$ with default $L = 2W$, and open strips [OS $W(\times L)$] with fully open boundary conditions (OBCs) and default $L = W$ [21].

TLH thermodynamics. In Fig. 2 we present our thermodynamical results from XTRG on cylinder (YC) and open geometries (OS), as defined earlier. In Fig. 2(a), we observe from YC5, OS6, and YC6 data that, besides a high-temperature round peak at $T_h \sim 0.55$, our YC data exhibit another peak (shoulder for OS6) at $T_l \sim 0.2$. On YCs, the peak position T_l stays nearly the same when increasing W from 5 to 6, also consistent with the shoulder in OS6 as well as in the experimental data. At the same time, the low-temperature peak becomes slightly weakened, yet towards the experimental data. When compared to the two virtually coinciding experimental data sets, YC6, TPO, earlier HTSE [5], and latest Padé [6,6] data [36] all agree well for $T \gtrsim T_h$ and reproduce the round peak of c_V at T_h.

The remarkable agreement of finite-size XTRG with experimental measurements can be ascribed to a short correlation length $\xi \lesssim 1$ lattice spacing for $T \gtrsim 0.4$ [21]. Deviations from experiments only take place below T_l, suggesting significant finite-size effects due to larger ξ in that regime. Moreover, we have checked the dependence of T_l on the cylinder length L for YC6, and find that the lower peak even gets slightly enhanced as L increases. In addition to YC and OS geometries, simulations on X cylinders also lead to the same scenario [21].

In Fig. 2(b), we present our data on thermal entropy, again directly juxtaposed with experimental as well as previous theoretical results. Whereas the YC5 data deviate at $T \lesssim 0.3$ due to finite-size effects, we observe good agreement between the two experimental data sets with our TPO results down to T_l, and with $W = 6$ data (OS6 and YC6) down to the lowest temperatures in the measurements. Notably, the thermal entropy per site S is about $1/3$ of the high-T limit, $S_\infty = \ln 2$,

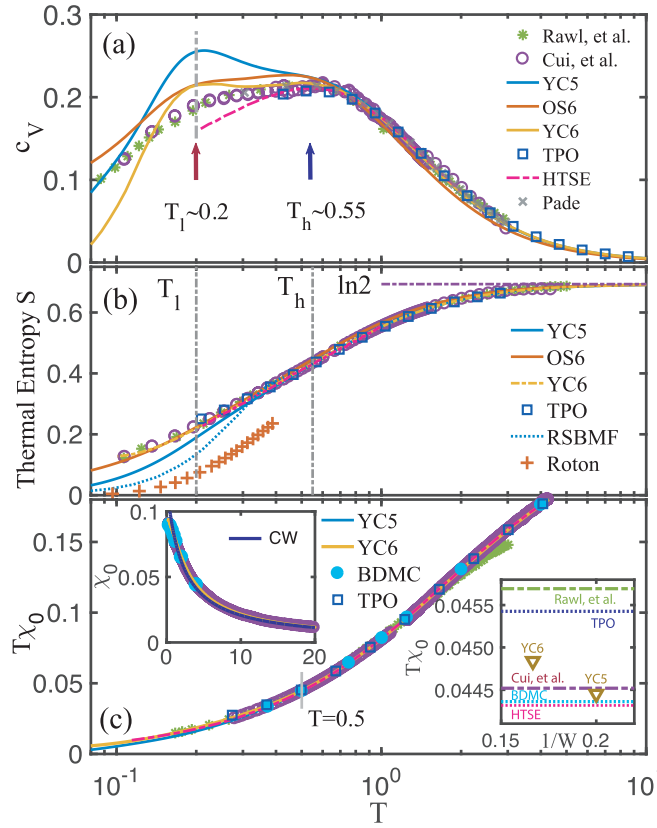

FIG. 2. Simulated thermodynamics in comparison to experimental measurements, Cui *et al.* (2018) [37] and Rawl *et al.* (2017) [36], as well as earlier numerical results. The YC and OS data are obtained via XTRG by retaining up to $D^* = 1000$ multiplets [$D \sim 4000$ U(1) states], and by a TPO method [21] on infinite lattices, keeping up to 40 bond states. (a) Specific heat, c_V, results benchmarked against HTSE [5,36] and experimental curves. (b) The thermal entropy S vs T, together with the reconstructed Schwinger boson mean field (RSBMF) [38], and "roton" contributions [16]. (c) Uniform magnetic susceptibility $T\chi_0$ vs T, shown with BDMC data [7]. The left top inset compares χ_0 to Curie-Weiss (CW) $\chi_0 = C/(T + \theta)$ in a wide temperature range, where $C = 1/4$ and $\theta = 2.06$. In the right bottom inset we further compare various $T\chi_0$ values at $T = 0.5$. The magnetic moment per Co is assumed $\simeq 2\mu_B$, with Landé factor $g \simeq 4.13$ [37].

at temperatures as low as $T \simeq 0.2$ where, for comparison, for SLH S is almost zero at the same temperature [6]. We emphasize that Fig. 2(b) is a direct comparison without any fitting, since the only parameter J has also been determined and thus fixed as 1.66 K in the experiments [36,37]. Nevertheless, since the experimental data of S are determined by integrating c_V/T, starting from the lowest accessible temperature T_x, systematic vertical shifts for the curves from Refs. [36,37] are necessary to reach the known large-T limits. This results in the residual entropies of $S(T_x) = 0.045$ and 0.06 at temperatures $T_x = 0.06$ and 0.08 K, for Refs. [36,37], respectively. Note that the large entropy due to quantum frustration at low T is not properly described in previous theories, e.g., RSBMF [38,39] as shown in Fig. 2(b).

Figure 2(c) presents our results for the average magnetic susceptibility. Both data sets, YC5 and YC6, agree

quantitatively with the experimental results, as well as HTSE data [5], from high temperatures down to $T \lesssim 0.1$, well beyond state-of-the-art BDMC results that reach down to $T = 0.375$ [7]. In the left top inset of Fig. 2(c), we also include a Curie-Weiss (CW) fit for $T \gtrsim 1$, resulting in the positive Weiss constant $\theta \approx 2J$. In the right bottom inset, we compare the $T\chi_0$ value at $T = 0.5$, and find the various numerical and experimental results all agree, up to three significant digits.

Two-temperature scales. As schematically depicted in Fig. 1, we uncover a two-temperature-scale scenario in the TLH. This confirms that the 120° order plus magnon excitations is not sufficient to describe TLH thermodynamics. References [40,41] argued that the TLH also has an additional type of excitations which are gapped, with the minimum of their quadratic dispersion at finite momentum, and referred to these as "rotonlike excitations" (RLEs), since their dispersions are reminiscent of that known for vortexlike excitations in He^4 [42]. Excitations with this type of dispersion have recently also been observed in neutron scattering experiments of TLH materials [43,44]. RLEs evidently play an important role in the intermediate-temperature regime in Fig. 1, but their precise nature has not yet been fully elucidated.

RLEs, although missed in the linear spin-wave theory, can be well captured by including $1/S$ corrections in calculating the magnon dispersions [41,45,46] and dynamical correlations [47,48]. Other proposals have also been put forward to understand RLEs, including the vortex-antivortex excitation [49] with signatures already in the classical TLH phase diagram versus finite temperature [50–53], (nearly deconfined) spinon-antispinon pair [16,40,54], and magnon-interaction-stabilized excitations [47,55,56].

First, the RLE quadratic band with a finite gap $\Delta \sim 0.55J$ contributes to a very prominent peak in the density of states around Δ [16]. This coincides with the high-temperature scale $T_h \sim \Delta$ here. Therefore a possible connection of RLEs to the thermodynamic anomaly in TLH has been suggested earlier [16,46]. Second, the RLEs themselves only start to significantly contribute to the entropy above T_l ["Roton" entry in Fig. 2(b), with data taken from Ref. [16]]. This suggests that the RLEs are activated in the intermediate temperature regime, i.e., $T_l \lesssim T \lesssim T_h$. Consequently, the onset of incipient magnetic order is postponed to a clearly lower temperature $T_l \sim 0.2$, which is remarkably close to previous HTSE studies, where $E_{\mathrm{RC}} \sim 0.2J$ sets the energy scale of classical correlation [5] as discussed earlier.

Spin structure factors. In order to shed light into the spin configurations across the intermediate regime, we turn to the temperature-dependent static structure factor, $S(q) \equiv \sum_j e^{-iq\cdot r_{0j}} \langle \mathbf{S}_0 \cdot \mathbf{S}_j \rangle_T$, where $r_{0j} \equiv r_j - r_0$ with r_j the lattice location of site j, and $S(q) \in \mathbb{R}$ due to lattice inversion symmetry. There are two further high-symmetry points of interest, $q = K$ and M, as marked in Fig. 3(a). Up to symmetric reflections, $K \equiv (\frac{2\pi}{3}, \frac{2\pi}{\sqrt{3}})$ relates to 120° noncollinear order, whereas $M \equiv (0, \frac{2\pi}{\sqrt{3}})$ relates to nearest-neighbor (stripe) AF correlations. The latter have also been related to RLEs which feature band minima at the M points [40,41,57].

In Figs. 3(a)–3(d) we show the overall landscape of $S(q)$. With decreasing temperature, $S(q)$ changes from rather featureless in Fig. 3(a), to showing bright regions in the vicinity

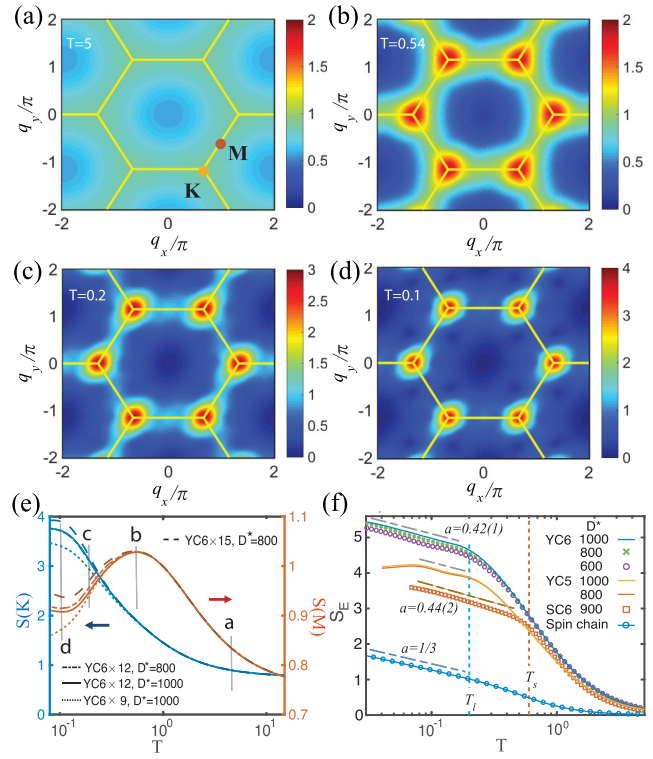

FIG. 3. (a)–(d) Structure factor on YC6 × 12 lattice, i.e., with q_y pointing along the direction of the cylinder, at temperatures $T = 5$, 0.54, 0.2, and 0.1, respectively, [vertical gray lines in (e)]. (e) $S(q)$ vs T at momenta $q = K$ and M where the legend holds for both data sets. (f) S_E vs T, where the tilted dashed lines indicate the logarithmic scaling $S_E = a\ln(\beta) + b$, where the slopes a seen for the TLH are similar to that for the SLH (SC6 data). The vertical dashed line labels the low-temperature scale $T_l \sim 0.2$ for TLH and the only temperature scale $T_s \sim 0.6$ for SLH. SC6 × 12 stands for a $W = 6, L = 12$ square cylinder, and S_E scaling in the Heisenberg chain (length $L = 200$) is also plotted as a comparison.

of the six equivalent K points as well as enhanced intensity at the M points at $T \sim T_h$ in Fig. 3(b). Even at $T \sim T_l$ in Fig. 3(c), one can still recognize an enhanced intensity $S(M)$, which fades out eventually when T is decreased below T_l in Fig. 3(d). A quantitative comparison is given in Fig. 3(e).

From Fig. 3(e), we observe that $S(K)$ increases monotonously as T decreases. It is featureless around T_h, and eventually saturates at the lowest T due to finite system size. For $T > T_l$, $S(K)$ increases only slowly with decreasing temperature, and is independent of length L. It therefore shows no signature of incipient order there. For $T < T_l$, $S(K)$ rapidly increases, which eventually saturates with decreasing T in an L-dependent manner, due to finite-size effects.

Furthermore, we observe from Fig. 3(e) that $S(M)$ develops a well-pronounced maximum around T_h. The maximum is already stable with system size, hence can be considered a feature in the thermodynamic limit. This is consistent with a picture that RLEs are activated near the M points.

MPO entanglement. The two-energy-scale scenario also leaves a characteristic trace in the entanglement entropy S_E, computed at a bond (near the center) of the MPO [20,58,59]. Gapless low-energy excitations in 1+1D conformal field theory (CFT) can give rise to a logarithmic increase of the

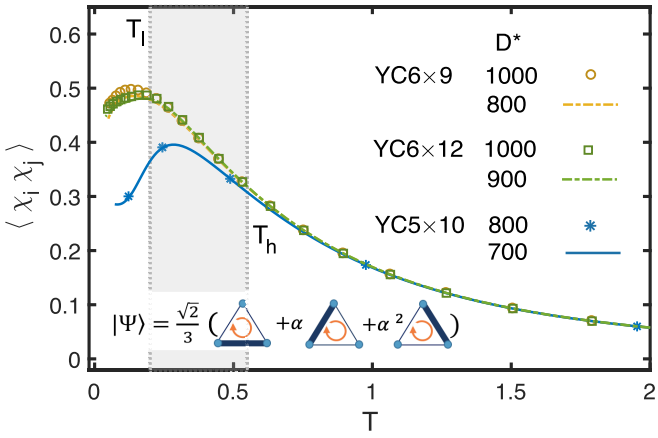

FIG. 4. Chiral correlations on cylinders, YC5 and YC6 (for YC4, see Ref. [21]). The inset represents the eigenstates Ψ (and Ψ^*) of the chiral operator χ (Fig. 1) with nonzero eigenvalues $\pm\sqrt{12}$. They have total spin $S = 1/2$, and hence are superpositions of configurations with two-site singlet dimers (thick lines) whose signs are fixed in clockwise order (arrow). Having $\alpha = \exp(2\pi i/3)$, this demonstrates the chiral nature.

entanglement, $S_E \propto -\frac{c}{3}\ln T$ with c the conformal central charge [20,60,61]. One can also observe logarithmic S_E behavior in the 2D SLH model, related to the spontaneous SU(2) symmetry breaking (at $T = 0$) [20], as also added for reference ("SC6" data) in Fig. 3(f).

We find similar behavior of the S_E profiles of the TLH on YC5 and YC6 geometries in Fig. 3(f) down to $T = 0.04$, with bond dimension $D^* \lesssim 1000$ multiplets ($D \sim 4D^*$ states). Interestingly, the lower-energy scale $T_l \sim 0.2$ (vertical dashed line) signals the onset of logarithmic entanglement scaling versus T, which, in agreement with Fig. 2(a), already coincides for $W = 5$ and 6. For YC5, the window with logarithmic entanglement is rather narrow, below of which S_E saturates as we already approach the ground state. For YC6, the entanglement continues to increase down to our lowest temperature $T = 0.03$. We associate the logarithmic S_E behavior with the onset of incipient order, which is closely related to SU(2) symmetry breaking at $T = 0$ that gives rise, e.g., to a $1/(N = LW)$ level spacing in the low-energy tower of states [2]. Concomitantly, we also observe a qualitative change of behaviors in the entanglement spectra at T_l [21].

Scalar chiral correlations. Chiral correlations in the TLH have raised great interest since the proposal of a Kalmeyer-Laughlin chiral spin liquid [62]. Intriguingly, recent $T = 0$ studies on the fermionic triangular-lattice Hubbard model proposed a chiral intermediate phase versus Coulomb repulsion which thus breaks time reversal symmetry [63]. While debated [64], we take this as a strong motivation to also study traces of chiral correlations in the TLH at finite T.

In Fig. 4, we present the chiral correlation $\langle\chi_i\chi_j\rangle$ between two nearest-triangles i, j in the system center, as defined with Fig. 1. This shows that chiral correlations are weak in both high- and low-temperature limit, while they become strong [63] in the intermediate-temperature regime, with a peak around T_l. Below T_l, the chiral correlations drop strongly, giving way to the buildup of coplanar incipient order.

Discussion. Our study suggests a tight connection between RLEs and chiral correlations in the intermediate regime $T_l \lesssim T \lesssim T_h$ (cf. Fig. 4). In this sense, we speculate that RLEs activated in the intermediate-temperature regime indicate phase-coherent rotating dimers, as schematically sketched with Fig. 4. Given that the complex phase of the dimers "rotates" by 2π, this suggests a possible link to a topological, vortexlike nature of the RLEs. Moreover, it resembles Feynman's notion of rotons in terms of quantized vortices in He^4 [42] via an exact mapping of TLH to a system of hardcore bosons. The latter further underlines the striking analogy between the anomalous thermodynamics of the TLH and the renowned roton thermodynamics in He^4 [65,66].

The low-energy scale T_l can be tuned by deforming the Hamiltonian, e.g., by altering the level of frustration by adding a next-nearest J_2 coupling to the TLH. We see that increasing J_2 reduces T_l, as well as the height of the corresponding peak in the specific heat, suggesting that the RLE gap is decreasing and the influence can thus spread down to even lower-temperature/energy scales, in consistency with dynamical studies of the J_1-J_2 TLH [67,68]. In addition, TLH can be continuously deformed into the SLH, where T_l increases and eventually merges with T_h once sufficiently close to the SLH. We refer more details to the Supplemental Material [21].

Outlook. A detailed study of the microscopic nature of RLEs, e.g., via dynamical correlations at finite temperature, is beyond the scope of the present Rapid Communication, and is thus left for future research. Further stimulating insights and possible superfluid analogies are also expected from an analysis of the interplay of external magnetic fields and thermal fluctuations in TLH [69,70] with clear experimental relevance [37].

Acknowledgments. W.L. and L.C. would like to thank Yi Cui and Wei-Qiang Yu for providing their original data of $Ba_8CoNb_6O_{24}$. W.L. is indebted to Lei Wang, Zi Cai, Hong-Hao Tu, Zheng-Xin Liu, Xue-Feng Zhang, Bruce Normand, and Jie Ma for stimulating discussions. This work was supported by the National Natural Science Foundation of China (Grants No. 11504014, No. 11834014, and No. 11874078) and supported by the Deutsche Forschungsgemeinschaft (DFG, German Research Foundation) under Germany's Excellence Strategy–EXC-2111–390814868. B.-B.C. was supported by the German Research foundation, DFG WE4819/3-1. A.W. was supported by the U.S. Department of Energy, Office of Basic Energy Sciences, under Contract No. DE-SC0012704. W.L. and S.-S.G. were supported by the Fundamental Research Funds for the Central Universities.

[1] P. W. Anderson, Resonating valence bonds: A new kind of insulator? Mater. Res. Bull. **8**, 153 (1973).

[2] B. Bernu, C. Lhuillier, and L. Pierre, Signature of Néel Order in Exact Spectra of Quantum Antiferromagnets on Finite Lattices, Phys. Rev. Lett. **69**, 2590 (1992).

[3] L. Capriotti, A. E. Trumper, and S. Sorella, Long-Range Néel Order in the Triangular Heisenberg Model, Phys. Rev. Lett. **82**, 3899 (1999).

[4] S. R. White and A. L. Chernyshev, Néel Order in Square and Triangular Lattice Heisenberg Models, Phys. Rev. Lett. **99**, 127004 (2007).

[5] N. Elstner, R. R. P. Singh, and A. P. Young, Finite Temperature Properties of the Spin-1/2 Heisenberg Antiferromagnet on the Triangular Lattice, Phys. Rev. Lett. **71**, 1629 (1993).

[6] N. Elstner, R. R. P. Singh, and A. P. Young, Spin-1/2 Heisenberg antiferromagnet on the square and triangular lattices: A comparison of finite temperature properties, J. Appl. Phys. **75**, 5943 (1994).

[7] S. A. Kulagin, N. Prokof'ev, O. A. Starykh, B. Svistunov, and C. N. Varney, Bold Diagrammatic Monte Carlo Method Applied to Fermionized Frustrated Spins, Phys. Rev. Lett. **110**, 070601 (2013).

[8] N. D. Mermin and H. Wagner, Absence of Ferromagnetism or Antiferromagnetism in One- or Two-Dimensional Isotropic Heisenberg Models, Phys. Rev. Lett. **17**, 1133 (1966).

[9] S. Chakravarty, B. I. Halperin, and D. R. Nelson, Low-Temperature Behavior of Two-Dimensional Quantum Antiferromagnets, Phys. Rev. Lett. **60**, 1057 (1988).

[10] S. Chakravarty, B. I. Halperin, and D. R. Nelson, Two-dimensional quantum Heisenberg antiferromagnet at low temperatures, Phys. Rev. B **39**, 2344 (1989).

[11] B. B. Beard, R. J. Birgeneau, M. Greven, and U.-J. Wiese, Square-Lattice Heisenberg Antiferromagnet at Very Large Correlation Lengths, Phys. Rev. Lett. **80**, 1742 (1998).

[12] J.-K. Kim and M. Troyer, Low Temperature Behavior and Crossovers of the Square Lattice Quantum Heisenberg Antiferromagnet, Phys. Rev. Lett. **80**, 2705 (1998).

[13] N. Elstner, A. Sokol, R. R. P. Singh, M. Greven, and R. J. Birgeneau, Spin Dependence of Correlations in Two-Dimensional Square-Lattice Quantum Heisenberg Antiferromagnets, Phys. Rev. Lett. **75**, 938 (1995).

[14] M. Greven, R. J. Birgeneau, Y. Endoh, M. A. Kastner, B. Keimer, M. Matsuda, G. Shirane, and T. R. Thurston, Spin Correlations in the 2D Heisenberg Antiferromagnet $Sr_2CuO_2Cl_2$: Neutron Scattering, Monte Carlo Simulation, and Theory, Phys. Rev. Lett. **72**, 1096 (1994).

[15] R. R. P. Singh and D. A. Huse, Microscopic calculation of the spin-stiffness constant for the spin-1/2 square-lattice Heisenberg antiferromagnet, Phys. Rev. B **40**, 7247 (1989).

[16] W. Zheng, J. O. Fjærestad, R. R. P. Singh, R. H. McKenzie, and R. Coldea, Excitation spectra of the spin-$\frac{1}{2}$ triangular-lattice Heisenberg antiferromagnet, Phys. Rev. B **74**, 224420 (2006).

[17] P. Azaria, B. Delamotte, and D. Mouhanna, Low-Temperature Properties of Two-Dimensional Frustrated Quantum Antiferromagnets, Phys. Rev. Lett. **68**, 1762 (1992).

[18] W. Li, S.-J. Ran, S.-S. Gong, Y. Zhao, B. Xi, F. Ye, and G. Su, Linearized Tensor Renormalization Group Algorithm for the Calculation of Thermodynamic Properties of Quantum Lattice Models, Phys. Rev. Lett. **106**, 127202 (2011).

[19] B.-B. Chen, Y.-J. Liu, Z. Chen, and W. Li, Series-expansion thermal tensor network approach for quantum lattice models, Phys. Rev. B **95**, 161104(R) (2017).

[20] B.-B. Chen, L. Chen, Z. Chen, W. Li, and A. Weichselbaum, Exponential Thermal Tensor Network Approach for Quantum Lattice Models, Phys. Rev. X **8**, 031082 (2018).

[21] See Supplemental Material at http://link.aps.org/supplemental/10.1103/PhysRevB.99.140404 for more details of the thermal tensor network methods including the XTRG and TPO approaches (Sec. I), for thermal data on XC4 and XC6, including internal energy versus T, dependence of the low-temperature scale T_l on length L, entanglement spectroscopy, correlation length ξ vs T, as well as finite-T chiral correlations on YC4 (Sec. II), and for thermodynamics of the J_1-J_2 TLH and frustrated SLH models (Sec. III), which include Refs. [22–35].

[22] A. Weichselbaum, Non-Abelian symmetries in tensor networks: A quantum symmetry space approach, Ann. Phys. **327**, 2972 (2012).

[23] L. De Lathauwer, B. De Moor, and J. Vandewalle, A multilinear singular value decomposition, SIAM J. Matrix Anal. Appl. **21**, 1253 (2000).

[24] Z. Y. Xie, J. Chen, J. F. Yu, X. Kong, B. Normand, and T. Xiang, Tensor Renormalization of Quantum Many-Body Systems Using Projected Entangled Simplex States, Phys. Rev. X **4**, 011025 (2014).

[25] H. C. Jiang, Z. Y. Weng, and T. Xiang, Accurate Determination of Tensor Network State of Quantum Lattice Models in Two Dimensions, Phys. Rev. Lett. **101**, 090603 (2008).

[26] W. Li, J. von Delft, and T. Xiang, Efficient simulation of infinite tree tensor network states on the Bethe lattice, Phys. Rev. B **86**, 195137 (2012).

[27] J. Jordan, R. Orús, G. Vidal, F. Verstraete, and J. I. Cirac, Classical Simulation of Infinite-Size Quantum Lattice Systems in Two Spatial Dimensions, Phys. Rev. Lett. **101**, 250602 (2008).

[28] A. Weichselbaum and S. R. White, Incommensurate correlations in the anisotropic triangular Heisenberg lattice, Phys. Rev. B **84**, 245130 (2011).

[29] T. Jolicoeur and J. C. Le Guillou, Spin-wave results for the triangular Heisenberg antiferromagnet, Phys. Rev. B **40**, 2727 (1989).

[30] A. V. Chubukov, T. Senthil, and S. Sachdev, Universal Magnetic Properties of Frustrated Quantum Antiferromagnets in Two Dimensions, Phys. Rev. Lett. **72**, 2089 (1994).

[31] Z. Zhu and S. R. White, Spin liquid phase of the $S = \frac{1}{2}$ J_1-J_2 Heisenberg model on the triangular lattice, Phys. Rev. B **92**, 041105(R) (2015).

[32] W.-J. Hu, S.-S. Gong, W. Zhu, and D. N. Sheng, Competing spin-liquid states in the spin-$\frac{1}{2}$ Heisenberg model on the triangular lattice, Phys. Rev. B **92**, 140403(R) (2015).

[33] Y. Iqbal, W.-J. Hu, R. Thomale, D. Poilblanc, and F. Becca, Spin liquid nature in the Heisenberg J_1-J_2 triangular antiferromagnet, Phys. Rev. B **93**, 144411 (2016).

[34] S.-S. Gong, W. Zhu, J.-X. Zhu, D. N. Sheng, and K. Yang, Global phase diagram and quantum spin liquids in a spin-$\frac{1}{2}$ triangular antiferromagnet, Phys. Rev. B **96**, 075116 (2017).

[35] E. Manousakis, The spin-1/2 Heisenberg antiferromagnet on a square lattice and its application to the cuprous oxides, Rev. Mod. Phys. **63**, 1 (1991).

[36] R. Rawl, L. Ge, H. Agrawal, Y. Kamiya, C. R. Dela Cruz, N. P. Butch, X. F. Sun, M. Lee, E. S. Choi, J. Oitmaa, C. D. Batista, M. Mourigal, H. D. Zhou, and J. Ma, $Ba_3CoSb_2O_9$: A spin-$\frac{1}{2}$ triangular-lattice Heisenberg antiferromagnet in the two-dimensional limit, Phys. Rev. B **95**, 060412(R) (2017).

[37] Y. Cui, J. Dai, P. Zhou, P. S. Wang, T. R. Li, W. H. Song, J. C. Wang, L. Ma, Z. Zhang, S. Y. Li, G. M. Luke, B. Normand, T. Xiang, and W. Yu, Mermin-Wagner physics, (H, T) phase

diagram, and candidate quantum spin-liquid phase in the spin-$\frac{1}{2}$ triangular-lattice antiferromagnet $Ba_8CoNb_6O_{24}$, Phys. Rev. Mater. **2**, 044403 (2018).

[38] A. Mezio, L. O. Manuel, R. R. P. Singh, and A. E. Trumper, Low temperature properties of the triangular-lattice antiferromagnet: A bosonic spinon theory, New J. Phys. **14**, 123033 (2012).

[39] A. Mezio, C. N. Sposetti, L. O. Manuel, and A. E. Trumper, A test of the bosonic spinon theory for the triangular antiferromagnet spectrum, Europhys. Lett. **94**, 47001 (2011).

[40] W. Zheng, J. O. Fjærestad, R. R. P. Singh, R. H. McKenzie, and R. Coldea, Anomalous Excitation Spectra of Frustrated Quantum Antiferromagnets, Phys. Rev. Lett. **96**, 057201 (2006).

[41] O. A. Starykh, A. V. Chubukov, and A. G. Abanov, Flat spin-wave dispersion in a triangular antiferromagnet, Phys. Rev. B **74**, 180403(R) (2006).

[42] R. P. Feynman, Atomic theory of the two-fluid model of liquid helium, Phys. Rev. **94**, 262 (1954).

[43] J. Ma, Y. Kamiya, T. Hong, H. B. Cao, G. Ehlers, W. Tian, C. D. Batista, Z. L. Dun, H. D. Zhou, and M. Matsuda, Static and Dynamical Properties of the Spin-1/2 Equilateral Triangular-Lattice Antiferromagnet $Ba_3CoSb_2O_9$, Phys. Rev. Lett. **116**, 087201 (2016).

[44] S. Ito, N. Kurita, H. Tanaka, S. Ohira-Kawamura, K. Nakajima, S. Itoh, K. Kuwahara, and K. Kakurai, Structure of the magnetic excitations in the spin-1/2 triangular-lattice Heisenberg antiferromagnet $Ba_3CoSb_2O_9$, Nat. Commun. **8**, 235 (2017).

[45] A. L. Chernyshev and M. E. Zhitomirsky, Magnon Decay in Noncollinear Quantum Antiferromagnets, Phys. Rev. Lett. **97**, 207202 (2006).

[46] A. L. Chernyshev and M. E. Zhitomirsky, Spin waves in a triangular lattice antiferromagnet: Decays, spectrum renormalization, and singularities, Phys. Rev. B **79**, 144416 (2009).

[47] M. Mourigal, W. T. Fuhrman, A. L. Chernyshev, and M. E. Zhitomirsky, Dynamical structure factor of the triangular-lattice antiferromagnet, Phys. Rev. B **88**, 094407 (2013).

[48] C. Luo, T. Datta, Z. Huang, and D.-X. Yao, Signatures of indirect K-edge resonant inelastic x-ray scattering on magnetic excitations in a triangular-lattice antiferromagnet, Phys. Rev. B **92**, 035109 (2015).

[49] J. Alicea, O. I. Motrunich, and M. P. A. Fisher, Theory of the algebraic vortex liquid in an anisotropic spin-$\frac{1}{2}$ triangular antiferromagnet, Phys. Rev. B **73**, 174430 (2006).

[50] H. Kawamura, A. Yamamoto, and T. Okubo, Z_2-vortex ordering of the triangular-lattice Heisenberg antiferromagnet, J. Phys. Soc. Jpn. **79**, 023701 (2010).

[51] M. V. Gvozdikova, P. E. Melchy, and M. E. Zhitomirsky, Magnetic phase diagrams of classical triangular and kagome antiferromagnets, J. Phys.: Condens. Matter. **23**, 164209 (2011).

[52] L. Seabra, T. Momoi, P. Sindzingre, and N. Shannon, Phase diagram of the classical Heisenberg antiferromagnet on a triangular lattice in an applied magnetic field, Phys. Rev. B **84**, 214418 (2011).

[53] I. S. Popov, P. V. Prudnikov, A. N. Ignatenko, and A. A. Katanin, Universal Berezinskii-Kosterlitz-Thouless dynamic scaling in the intermediate time range in frustrated Heisenberg antiferromagnets on a triangular lattice, Phys. Rev. B **95**, 134437 (2017).

[54] B. Dalla Piazza, M. Mourigal, N. B. Christensen, G. J. Nilsen, P. Tregenna-Piggott, T. G. Perring, M. Enderle, D. F. McMorrow, D. A. Ivanov, and H. M. Rønnow, Fractional excitations in the square-lattice quantum antiferromagnet, Nat. Phys. **11**, 62 (2014).

[55] R. Verresen, F. Pollmann, and R. Moessner, Quantum dynamics of the square-lattice Heisenberg model, Phys. Rev. B **98**, 155102 (2018).

[56] R. Verresen, F. Pollmann, and R. Moessner, Strong quantum interactions prevent quasiparticle decay, arXiv:1810.01422.

[57] E. A. Ghioldi, M. G. Gonzalez, S.-S. Zhang, Y. Kamiya, L. O. Manuel, A. E. Trumper, and C. D. Batista, Dynamical structure factor of the triangular antiferromagnet: Schwinger boson theory beyond mean field, Phys. Rev. B **98**, 184403 (2018).

[58] F. Verstraete, J. J. García-Ripoll, and J. I. Cirac, Matrix Product Density Operators: Simulation of Finite-Temperature and Dissipative Systems, Phys. Rev. Lett. **93**, 207204 (2004).

[59] A. E. Feiguin and S. R. White, Finite-temperature density matrix renormalization using an enlarged Hilbert space, Phys. Rev. B **72**, 220401(R) (2005).

[60] T. Barthel, One-dimensional quantum systems at finite temperatures can be simulated efficiently on classical computers, arXiv:1708.09349.

[61] J. Dubail, Entanglement scaling of operators: A conformal field theory approach, with a glimpse of simulability of long-time dynamics in $1+1$D, J. Phys. A: Math. Theor. **50**, 234001 (2017).

[62] V. Kalmeyer and R. B. Laughlin, Equivalence of the Resonating-Valence-Bond and Fractional Quantum Hall States, Phys. Rev. Lett. **59**, 2095 (1987).

[63] A. Szasz, J. Motruk, M. P. Zaletel, and J. E. Moore, Observation of a chiral spin liquid phase of the Hubbard model on the triangular lattice: A density matrix renormalization group study, arXiv:1808.00463.

[64] T. Shirakawa, T. Tohyama, J. Kokalj, S. Sota, and S. Yunoki, Ground-state phase diagram of the triangular lattice Hubbard model by the density-matrix renormalization group method, Phys. Rev. B **96**, 205130 (2017).

[65] J. D. Wasscher, H. C. Kramers, and C. J. Gorter, The specific heat of liquid helium between 0.25 and 1.9 K, Physica **18**, 329 (1952).

[66] P. J. Bendt, R. D. Cowan, and J. L. Yarnell, Excitations in liquid helium: Thermodynamic calculations, Phys. Rev. **113**, 1386 (1959).

[67] E. A. Ghioldi, A. Mezio, L. O. Manuel, R. R. P. Singh, J. Oitmaa, and A. E. Trumper, Magnons and excitation continuum in XXZ triangular antiferromagnetic model: Application to $Ba_3CoSb_2O_9$, Phys. Rev. B **91**, 134423 (2015).

[68] F. Ferrari and F. Becca, Dynamical structure factor of the J_1-J_2 Heisenberg model on the triangular lattice: Magnons, spinons, and gauge fields, arXiv:1903.05691.

[69] C. Griset, S. Head, J. Alicea, and O. A. Starykh, Deformed triangular lattice antiferromagnets in a magnetic field: Role of spatial anisotropy and Dzyaloshinskii-Moriya interactions, Phys. Rev. B **84**, 245108 (2011).

[70] O. A. Starykh, Unusual ordered phases of highly frustrated magnets: A review, Rep. Prog. Phys. **78**, 052502 (2015).

Correction: The support statement for author A.W. required an update and has been fixed.